



**HAL**  
open science

## Spreading of water on a liquid-infused solid

Saurabh Nath, David Quéré

► **To cite this version:**

Saurabh Nath, David Quéré. Spreading of water on a liquid-infused solid. *Physical Review Fluids*, 2022, 7, 10.1103/physrevfluids.7.084003 . hal-03825433

**HAL Id: hal-03825433**

**<https://cnrs.hal.science/hal-03825433>**

Submitted on 22 Oct 2022

**HAL** is a multi-disciplinary open access archive for the deposit and dissemination of scientific research documents, whether they are published or not. The documents may come from teaching and research institutions in France or abroad, or from public or private research centers.

L'archive ouverte pluridisciplinaire **HAL**, est destinée au dépôt et à la diffusion de documents scientifiques de niveau recherche, publiés ou non, émanant des établissements d'enseignement et de recherche français ou étrangers, des laboratoires publics ou privés.

## Spreading of water on a liquid-infused solid

Saurabh Nath  and David Quéré 

*Physique et Mécanique des Milieux Hétérogènes, UMR 7636 du CNRS, PSL Research University, ESPCI, 75005 Paris, France*



(Received 28 December 2021; accepted 20 July 2022; published 29 August 2022; corrected 12 September 2022)

Liquid-infused solids (LISs) are textured materials infused by oil, which makes them highly slippery for drops of another nonmiscible liquid. In this article, we discuss what happens when a water drop contacts and spreads on such LISs. Focusing on the influence of the oil layer trapped in the texture, we report that, despite lubrication, spreading on a LIS is slower than on a bare solid, even at short times. Yet the dynamics unexpectedly preserves its scaling, which we explain by considering the friction in the film, showing that the slippery nature of LISs can be accompanied by a significant dissipation.

DOI: [10.1103/PhysRevFluids.7.084003](https://doi.org/10.1103/PhysRevFluids.7.084003)

### I. INTRODUCTION

The fate of a drop that contacts a solid has been the subject of many investigations, ranging from static problems (what is the final state of the liquid?) to dynamic questions (how does the liquid reach equilibrium?) [1,2]. For the common case of water droplets with millimetric size  $R$  deposited on solids they partially wet, the combination of limited spreading and low liquid viscosity makes the dynamical resistance mainly dominated by inertia [3–6]. This regime is followed by a relaxation toward equilibrium, where both pinning and viscous forces can play a role. The emergent dynamics is a short process on the whole, typically on the scale of a few milliseconds: seen with our naked eye, water drops deposited on plastic quasi-instantaneously form spherical caps.

Spreading is quantified by the law  $r = f(t)$ , denoting  $r$  as the radius of substrate-liquid contact and  $t$  as the time, which provides an estimate of the duration  $\tau \sim f^{-1}(R)$  of the process. As a drop initially spherical contacts a solid, a bridge forms and grows, and the dynamics of this junction results from an interplay between geometry and physics [4]. On the one hand, the lateral and vertical bridge dimensions  $r$  and  $\delta$  obey the Hertz scaling,  $r^2 \sim \delta R$ , that expresses the contact of a sphere with a plate. On the other hand, the vertical speed at which the spherical drop falls onto the solid plate is given by balancing inertia with surface tension, which yields a speed  $V$  scaling as  $(\gamma/\rho R)^{1/2}$ , where  $\gamma$  and  $\rho$  are the surface tension and density of the liquid [3]. Plugging the falling distance  $\delta \sim Vt$  into Hertz's relationship provides the inertial law of spreading:

$$r \sim (D_0 t)^{1/2}, \text{ with } D_0 = (\gamma R / \rho)^{1/2} \quad (1)$$

This regime holds at short time ( $t < \rho R^2 / \eta$ ), and it is thus particularly relevant when the liquid viscosity  $\eta$  is low, as it is for water. This “diffusive” law has been found to be universal (that is, independent of the solid properties) and obeyed for fully and partially wetted surfaces, as well as for chemically patterned, soft, and complex materials [3–6]. Equation (1) provides an estimate of the typical spreading time in situations of partial wetting, where the liquid meets the solid with a contact angle  $\theta$  so as to form a lens with radius  $R \sin \theta \sim R$ . Hence the typical spreading time  $\tau$  scales as  $R^2 / D_0$ , that is, as  $(\rho R^3 / \gamma)^{1/2}$  with a prefactor a function of  $\theta$ .  $\tau$  is expected to be a few milliseconds for millimetric drops, in agreement with the observations [3–6]. All these arguments should be valid for contact angles on the order of  $90^\circ$ : for more acute angles, the dynamics of

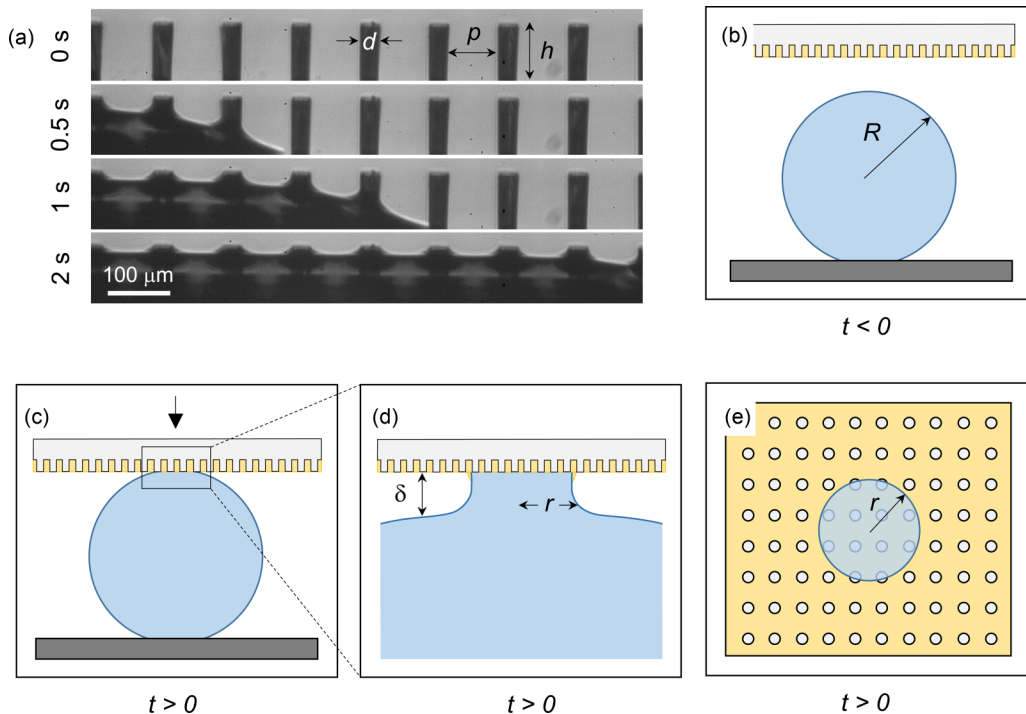


FIG. 1. (a) Liquid-infused solids (LISs) are prepared by contacting a texture (here with a height  $h = 90 \mu\text{m}$ ) with silicone oil (viscosity  $\eta_o = 19 \text{ mPa s}$ ). The oil invades the texture and fills its cavities. (b) Sideview sketch of our experimental setup: a water droplet sitting on a superhydrophobic solid is approached from the top by a transparent LIS. (c) At  $t = 0$ , the drop is brought in contact with the infused surface on the top. (d) Simplified geometry of the contact with dimensions  $r$  and  $\delta$  as the drop starts to spread. (e) Top view sketch of the water contact seen through the transparent infused material.

spreading becomes sensitive to viscous dissipation close to the contact line, which dramatically slows the motion (Tanner's law) [7].

Here we revisit this classical problem by considering spreading of water on liquid-infused solids (LISs), namely, textured materials infused by an oil. As shown in Fig. 1(a), we prepare such solids by wicking a silicone oil within a forest of micropillars. LISs have special dynamical properties, in particular because the liquid trapped in the texture lends them liquidlike properties, with little adhesion and a slippery character towards other liquids or even solids [8–12]. However, drops moving on LISs (under the action of gravity, for instance) are known to be slowed by a stationary meniscus of lubricant surrounding the moving drop [10–12]. We wonder if the universality of the spreading law, as expressed by Eq. (1), holds for drops spreading on infused surfaces as well or if it is affected by the presence of the infusion.

## II. FABRICATION

Capturing the early dynamics of a solid-liquid contact requires simultaneous lateral and vertical views and thus the use of transparent LISs [13]. Such materials are made in a few steps. We first start by spin coating a layer of SU-8 resin on a clean, dehydrated silicon wafer, and control the resin thickness by the speed of rotation. We then shine UV light through a mask comprising square arrays of circular pillars. Thereafter a PDMS countermold of the SU-8 texture is made from which we achieve a mold with a transparent optical adhesive (Norland Optical Adhesive) on a glass slide

[13,14]. The obtained transparent microtextured surface is finally infused with silicone oil, whose optical index is comparable to that of the resin, leading to a better transparency.

Just infusing oil inside the texture does not provide slippery surfaces, due to the edges at the pillar tops [15]. This can be fixed by adding a second scale of roughness, which we do by drawing the textured substrate from a dilute suspension of hydrophobic nanobeads (Glaco Mirror Coat, Soft 99) [16]. After drying the solvent at 70 °C for 30 min, the beads ( $\sim 30$  nm) coat both the substrate and the pillars without altering transparency. The process is repeated three times to ensure uniformity of the nanobead coating. Infusion itself is performed by keeping the substrate vertical and contacting silicone oil. Hence oil wicks only between the pillars and within the nanobead cavities, which ensures that we do not overinfuse the material, yet make it highly slippery for water (roll-off angle of  $\sim 1^\circ$  for water drops of  $20 \mu\text{l}$ ).

### III. THE EXPERIMENT

A spreading experiment is schematized in Figs. 1(b)–1(e). Our substrates (top of the figure) have micropillars with density  $\phi = 23\%–25\%$ , height  $h = 20 \pm 3 \mu\text{m}$ , lateral size  $d = 18 \mu\text{m}$ , and spacing  $p = 15 \mu\text{m}$ . The lubricant is a silicone oil with surface tension  $\gamma_o = 20 \text{ mN/m}$  and viscosity  $\eta_o$  ranging from 5 mPa s to 1000 mPa s. Millimeter-sized drops (in blue in the figure) are made of water, with surface tension  $\gamma = 72 \text{ mN/m}$  and viscosity  $\eta = 1 \text{ mPa s} \ll \eta_o$ . We start by placing a drop on a Glaco-treated superhydrophobic glass slide (dark gray in the figure), which preserves its sphericity and allows us to study spreading without impact, as would necessarily happen if drops were directly released on the infused material. Instead, we approach at small speed (about  $50 \mu\text{m/s}$ ) the LIS from the top, with its infused side facing downward. Two high-speed cameras simultaneously image the contact with top-down (with 400 000 fps) and side views (with 5000 fps), using respective backlighting at the bottom and on the side.

For the purposes of analyzing the early time evolution of the substrate-liquid radius, we exclusively use the top-down data, which are less prone to error than sideview, as shown in previous works [5,6]. The experiment is repeated multiple times for droplet volumes ranging from 1 to  $40 \mu\text{l}$  and for six oil viscosities, namely, 5, 19, 48, 96, 485, and 970 mPa s. A separate set of experiments is performed after replacing the infused surface by silanized hydrophobic glass of similar wetting properties, so as to extract the specific contribution of infusion in the contact dynamics. We provide in Figs. 2(a) and 2(b) three top views of the growing contact at early times and graphs of the evolution of the water contact radius with  $R = 0.65 \pm 0.05 \text{ mm}$ .

The views reveal unusual features, in particular a loss of universality: even at short time, where inertia is expected to dominate viscous effects, the dynamics depends on the viscosity of the oil infusing the texture: the more viscous the oil, the slower the spreading. Other original behaviors are evidenced by plotting the contact radius  $r$  as a function of time [Figs. 2(b) and 2(c)]. The data at low oil viscosity are close to that on a solid, while water spreads slower on the more viscous oil, a case we could have thought solidlike. The influence of the viscosity is also noticeable in some details of the spreading: water being more mobile on the less viscous oil, equilibrium is approached with oscillations of the contact radius; in contrast, spreading at larger oil viscosity shows steps (especially visible for  $\eta_o = 96 \text{ mPa s}$  and further discussed in the Supplemental Material [17]) that correspond to the spacing  $p + d = 33 \mu\text{m}$  of the subjacent network. Finally, all data become similar at “long” time, the wetting properties of silicone oil being nearly independent of the oil viscosity, and comparable to that of silanized solid surfaces.

Despite these differences, a common scaling emerges when plotting the LIS data in a logarithmic graph [Fig. 2(c)]. In a range of about two decades in time, all data follow a  $t^{1/2}$  dynamics (solid lines in the inset) before reaching equilibrium at large time. This constitutes our main result. We also notice several features: first, data start to deviate from the half line around 0.7–1.1 ms, which is the inertio-capillary timescale  $(\rho R^3/\gamma)^{1/2}$  of the drop. This also happens to be the typical time required for the capillary wave generated by the drop upon contact to reach the farthest point from contact, creating a shift in momentum, and transiently arresting the spreading. We further note that

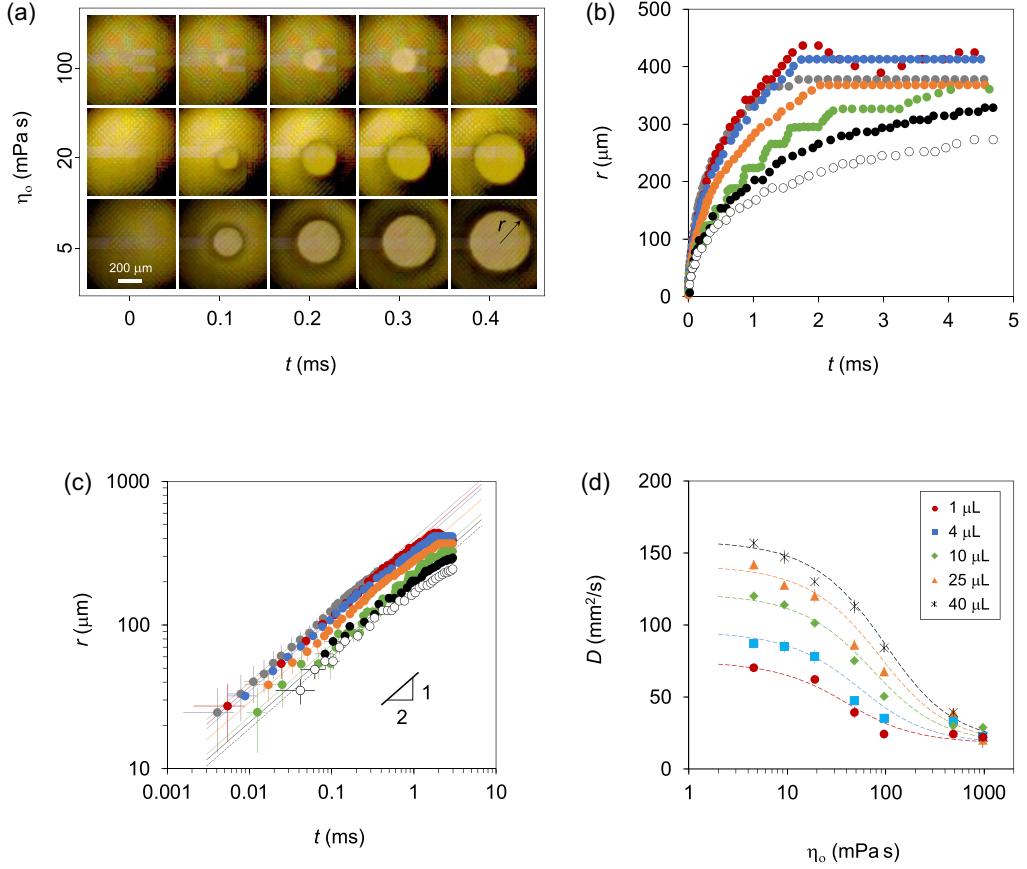


FIG. 2. (a) Time-lapse top-down images of the contact between a water drop (radius  $R = 0.65$  mm) and a LIS, for three different oil viscosities:  $\eta_o = 5$ , 19, and 96 mPa s. (b) Time evolution  $r(t)$  of the radius of contact between water and a hydrophobic solid (gray data) or a LIS with  $\eta_o = 5$  mPa s (red data),  $\eta_o = 19$  mPa s (blue data),  $\eta_o = 48$  mPa s (orange data),  $\eta_o = 96$  mPa s (green data),  $\eta_o = 485$  mPa s (black data), and  $\eta_o = 970$  mPa s (white data). (c) In logarithmic scales, the same plot reveals a diffusive-type behavior for all substrates (slope  $1/2$ ). Error bars in time correspond to one standard deviation equal to the inverse of the frames per second and error bars in length correspond to one standard deviation equal to one-pixel size. (d) Effective diffusivity  $D$  extracted from (c) as a function of the viscosity  $\eta_o$  of the infusing oil, at fixed water volumes:  $\Omega = 1 \mu\text{l}$  (circles),  $\Omega = 4 \mu\text{l}$  (squares),  $\Omega = 10 \mu\text{l}$  (diamonds),  $\Omega = 25 \mu\text{l}$  (triangles),  $\Omega = 40 \mu\text{l}$  (asterisks).

the steps at large  $\eta_o$  do not modify the diffusive-like behavior, as also known when a liquid invades a forest of micropillars [18].

The  $t^{1/2}$  dynamics was established for the spreading of nonviscous liquids on regular solids [Eq. (1)] and found to be universal—which it is here from the exponent point of view, but not for the “diffusivity”  $D$ , which raises a stimulating question: how can the oil modify the dynamics without affecting its scaling? Furthermore, the variation of the diffusivity with oil viscosity needs to be explained. Figure 2(d) shows that  $D$  [as extracted by fitting  $r(t)$  to  $r^2 = 2Dt$ ] decreases with  $\eta_o$  for all tested volumes. First ( $\eta_o < \eta_1 \approx 1\text{--}10$  mPa s), the function  $D(\eta_o)$  tends to plateau at values that increase with volume, as expressed in Eq. (1). At larger  $\eta_o$ ,  $D$  decreases rapidly with the oil viscosity, as seen in Fig. 2(a), even if the diffusivities at large viscosity ( $\eta_o > \eta_2 \approx 100$  mPa s) seem to converge to a value independent of the drop volume.

## IV. THE MODEL

We first discuss the force driving the spreading. As water advances on the LIS, the nature and areas of the interfaces change, and different cases are possible, depending, for instance, on the possibility of oil cloaking water or not [10]. For the sake of simplicity, we consider that water essentially moves on oil, a reasonable statement for a dilute texture: the top surface of a highly slippery LIS is essentially oily. In the first steps of the spreading, the spherical drops of water (radius  $R$ ) develop a contact with horizontal and vertical dimensions  $r$  and  $\delta$ , as sketched in Figs. 1(c)–1(e). The driving Laplace pressure in the contact region scales as  $\gamma/\delta$ , which classically provides a driving force  $\gamma r$ , once integrated over the lateral surface area  $r\delta$  of the contact. If oil cloaks the drop, surface tension becomes the sum of water-oil and oil-water tensions, on the same magnitude as  $\gamma$ , so that we generically consider  $\gamma r$  as the spreading force.

As already discussed, the first natural cause of resistance at short times is inertia. For a bridge with volume  $r^2\delta$ , the inertial force scales as  $\rho(r^2\delta)V^2/r \sim \rho r^3 V^2/R$ . If we balance it with the driving force, we get the diffusive-type dynamics for the bridge expansion described in Eq. (1). Such dynamics is independent of the oil viscosity, a feature consistent with our observation at small  $\eta_o$ . In addition, the dynamics is expected to vary with the drop volume  $\Omega$ , as  $\Omega^{1/6}$ , in agreement with Fig. 2(d) where the coefficient  $D$  increases by a factor of order 2 when the volume is multiplied by 40.

However, we also report an influence of the oil viscosity, which becomes significant above a characteristic value  $\eta_1$  on the order of 10 mPa.s. The origins of viscous dissipation are multiple. First, the water drop could be surrounded by an oil meniscus, as it is when such a drop runs down an inclined LIS [10–12,15]. We can associate a “line friction” to this meniscus that scales, per unit length, as  $\beta(\eta_o V/\theta)$ , where  $\beta$  is a numerical factor accounting for the singular dissipation in the liquid wedge [18]. The dynamic contact angle  $\theta$  is given by Tanner’s law,  $\theta \sim (\beta\eta_o V/\gamma)^{1/3}$ , which yields a friction scaling as  $\gamma_o r (\beta\eta_o V/\gamma_o)^{2/3}$  after integrating the force over the contact line. Its balance with the spreading force  $\gamma r$  provides a constant speed of spreading inversely proportional to the oil viscosity—two facts inconsistent with the observations, where we report neither a linear relation between the bridge size and time nor such strong dependency on the oil viscosity.

In our experiment, water flows on a composite material made of solid and oil, which raises the question of the boundary condition at the water-oil interface. An oil with low viscosity is expected to lubricate water, so that the velocity at the water-oil interface can be of order  $V$ . This contrasts with the case of a viscous oil, for which we expect an immobile oil-water interface, a point further discussed (see the next section and the Supplemental Material [17]). Oil sheared by the spreading water dissipates energy. At low pillar density, the corresponding friction can be reduced to that of a liquid flowing in a gap with thickness  $h$ , that is,  $(\eta_o V/h)r^2$ . This form becomes more complex when pillars are denser, and then it involves the pillar diameter  $d$  and mutual distance  $p$ , as shown by Hasimoto *et al.* [19,20]. However, it reduces to the expression we used for our archetypal texture where all distances  $h$ ,  $p$ , and  $d$  are comparable. When balanced with the driving force  $\gamma r$ , it yields a new diffusive-type law:

$$r^2 \sim D_1 t, \text{ with } D_1 = \gamma h/\eta_o. \quad (2)$$

Hence dissipation in the oil film can generate a diffusive-type dynamics, in agreement with experiments [Fig. 2(c)]. The crossover (in viscosity) from the inertial to the viscous regime is found by comparing the diffusivities  $D_0$  and  $D_1$ , which provides a threshold oil viscosity  $\eta_1 \sim (\rho\gamma h^2/R)^{1/2}$  on the order of 1 mPa.s, consistent with our observations from Fig. 2(d). However, Fig. 2(d) shows that the variation of  $D(\eta_o)$  in the second regime is weaker than predicted by the scaling  $D_1 \sim 1/\eta_o$ . This can be understood by considering both kinds of diffusive dynamics, when inertia and viscous friction are of the same order. Dividing the inertial force  $\sim \rho(r^3/R)V^2$  by the viscous force in the film provides a Reynolds number,  $\text{Re} = \rho V r h/\eta_o R$  (where the quantity  $V r$  is independent of time), and confirms that inertia will dominate viscosity ( $\text{Re} \gg 1$ ) at low  $\eta_o$ . Treating viscous effects as a perturbation of the inertial regime, as suggested by Fig. 2, the number  $\text{Re}$  simply reduces to  $1/\psi$ ,

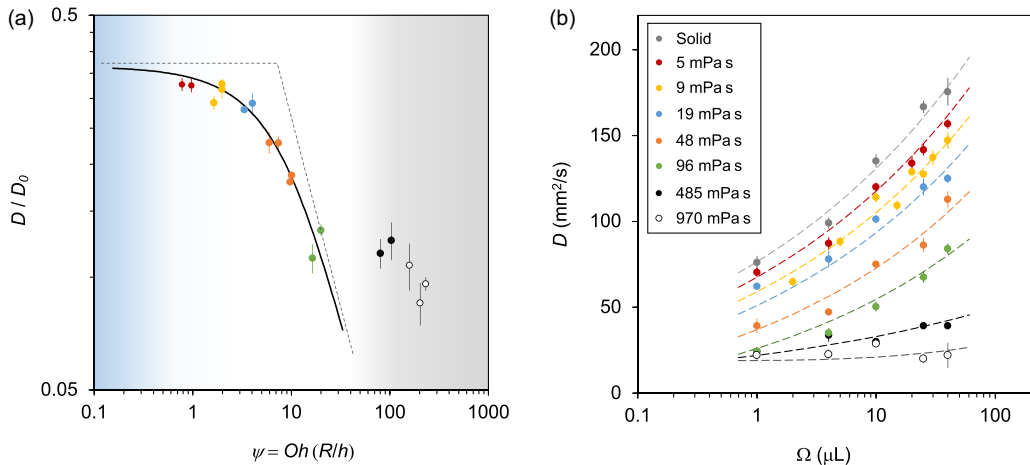


FIG. 3. (a) Effective diffusivity  $D$  of the spreading dynamics [normalized by that given by Eq. (1)] plotted against  $\psi = \eta_o R^{1/2} / h \rho^{1/2} \gamma^{1/2}$ , where we vary  $\psi$  by changing the oil viscosity from 5 to 970 mPa s and the drop volume from 1 to 4  $\mu\text{l}$  (quasispherical drops). The solid line gives the solution of Eq. (3), where we introduced two numerical coefficients  $\alpha \approx 2.8$  and  $\beta \approx 0.15$  (missing in our scaling arguments) in front of the quadratic and linear terms;  $\alpha$  is known from spreading on bare solids and  $\beta$  corresponds to the best fit of data. Dotted lines show the asymptotic inertial and viscous regimes. The blue and white regions respectively correspond to the inertial regime on a bare solid and to the visco-inertial regime described by Eq. (3); the gray shade is for the high-viscosity regime. The color scheme for the data is the same as in Figs. 2 and 3(b), corresponding to oil viscosities increasing from left to right. (b) Effective diffusivity for water drops as a function of their volume  $\Omega$  at a fixed  $\eta_o$ . The control case of a hydrophobic solid is plotted as gray data. The dotted lines serve as guides for the eye.

where  $\psi = \text{Oh}(R/h)$ , denoting  $\text{Oh} = \eta_o / (\rho \gamma R)^{1/2}$  as the Ohnesorge number. When  $\psi$  is of order unity, viscous effects can affect the inertial spreading even at early time and reveal an influence of the subjacent layer of oil. However, we expect that this influence will not modify the scaling of the dynamics, since both the inertial and the viscous resistance lead to  $t^{1/2}$  kinetics. If we balance them with the driving capillary force, we obtain a very simple equation for the quantity  $D$  that writes

$$D^2 + \psi D D_0 - D_0^2 \sim 0. \quad (3)$$

The general solution of Eq. (3) matches the two asymptotic limits described earlier. At small  $\psi$ , the latter equation reduced to  $D \sim D_0$  [Eq. (1)], that is, the behavior expected when inertia is dominant; at large  $\psi$ , the solution tends towards  $D \sim D_0 / \psi \sim D_1$  [Eq. (2)], the case where the effect of viscosity becomes dominant. These asymptotic laws are drawn with dotted lines in Fig. 3(a), where we add both the solution of Eq. (3) (solid line), where we introduced two numerical coefficients  $\alpha \approx 2.8$  and  $\beta \approx 0.15$  in front of the quadratic and linear terms;  $\alpha$  is known from spreading on bare solids and  $\beta$  corresponds to the best fit of data.

In the figure, the measured diffusivity is normalized by the inertial one  $D_0$  [Eq. (1)] and plotted as a function of  $\psi$ . We restrict the comparison between experiments and model to microlitric quasispherical drops ( $\Omega = 1 \mu\text{l}$  and  $\Omega = 4 \mu\text{l}$ ). As predicted by the model, Fig. 3(a) provides a collapse of all data, obtained by varying both the oil viscosity and the drop size. In addition, the solution of Eq. (3) (drawn with a solid line) nicely captures the observations at small and moderate values of  $\psi$ . We also notice deviations at large  $\psi$ , which we discuss in the next section. The oil viscosity is the main ingredient of the Ohnesorge number  $\text{Oh} = \eta_o / (\rho \gamma R)^{1/2}$ , while the drop size is included both in  $D_0$  and in  $\psi$ . The number  $\psi$  being of order unity in our experiments, most data lie in the crossover regime between the inertial and viscous ones. The fit provides the numerical

coefficients ignored in our scaling arguments: as seen from the asymptotic behaviors,  $D/D_0$  tends towards 0.36 at small  $\psi$ , the value found on a solid [Fig. 3(b) and Refs. [3] to [6]]; at large  $\psi$ , the fit is  $D/D_0 = 2.45/\psi$ , that is, Eq. (2) with a numerical factor that remains to be understood from a complete calculation of the dissipation in the oil film.

We assumed that the viscous dissipation in oil was larger in the film than in the meniscus, contrasting with other situations [15]. For a water drop moving on a LIS (owing to gravity, for instance), the friction in the meniscus generally exceeds that in the film, for two reasons. On the one hand, the stationary oil meniscus joins the substrate with an acute angle, which accentuates the dissipation; on the other hand, the speed (typically 0.1 to 10 mm/s) is much smaller than in spreading, which minimizes the film friction [21,22]. In our case, the oil meniscus is not stationary (it gradually builds when the bridge propagates), and it does not meet the substrate with an acute angle, since we discuss situations where contact is being established. Moreover, the liquid bridge grows at a large speed, typically 1 to 10 cm/s, compared to that of gravity-driven drops. It is known that drops on LISs moving faster than 1 cm/s exhibit a dynamically deformed meniscus and a completely different friction scaling, the physics of which has not yet been understood [15]. Hence, we do not expect *a priori* that the meniscus force would exceed the film friction for spreading drops. We can go further by comparing their amplitude.

Because the classical scaling of meniscus friction corresponds to acute angles, it overestimates (by far) the dissipation in an obtuse wedge. However, even if we consider this scaling and compare it to the expression in the film, we find that the film friction dominates only when the contact line radius  $r$  is larger than a distance scaling as  $\beta h^{3/2} \gamma^{1/2} / (\eta_o D)^{1/2}$ . For making the latter expression more explicit, we take the inertial diffusivity  $(\gamma R / \rho)^{1/2}$  as a scale for  $D$ , so that the previous relation can be rewritten as  $r > \beta h (\gamma_o / \gamma)^{1/4} / \psi^{1/2}$ . For our range of oil viscosities and droplet sizes,  $\psi$  is of order unity, so that the film friction should dominate the meniscus friction for a contact size  $r$  larger than a few times  $h$ , the typical distance where we start our measurements.

## V. DISCUSSION

We first discuss the regime of large oil viscosity. Figure 3(a) shows that the dynamics does not follow Eq. (3) anymore but reaches a minimum value smaller by a factor 3 to 4 compared to that on nonviscous oil. In this limit, we expect the velocity  $V_s$  at the oil-water interface to decrease, which reduces the influence of the oil viscosity. We obtain the “effective slip” velocity  $V_s$  at the oil-water interface from a balance of shear stress, that is,  $\eta_w (V - V_s) / \zeta \sim \eta_o V_s / h$ , where  $\zeta$  is the thickness of the viscous boundary layer within the drop. We deduce that  $V_s$  scales as  $V / (1 + \eta_o \zeta / \eta_w h)$ , an expression that quantifies how slip vanishes when increasing  $\eta_o$ . As proposed in the context of coalescence [23], we consider  $\gamma / \eta_w$  as a typical velocity just after contact and evaluate  $\zeta$  from a balance of inertia with viscosity,  $\rho (\gamma / \eta_w)^2 \sim \eta_w (\gamma / \eta_w) / \zeta$ , which yields  $\zeta \sim \eta_w^2 / \rho \gamma$  [23]. This distance is smaller than the drop size  $R$  if  $\eta_w$  is smaller than  $(\rho \gamma R)^{1/2}$ , around 10 mPa s for millimetric drops [24]. The shear stress balance thus becomes explicit, with a slip velocity  $V_s \sim V / (1 + \eta_w \eta_o / \rho \gamma h)$ .

This expression implies the existence of a second critical oil viscosity  $\eta_2 \sim \rho \gamma h / \eta_w$ , around 100 mPa s. For  $\eta_o < \eta_2$ , we recover the regime of pure slip ( $V_s \sim V$ ) discussed earlier. At higher oil viscosity ( $\eta_o > \eta_2$ ), the velocity  $V_s \sim V (\rho \gamma h / \eta_w \eta_o)$  is all the more reduced as  $\eta_o$  increases. The dissipation force  $(\eta_o V_s / h) r^2$  then scales as  $(\rho \gamma / \eta_w) V r^2$ . When balanced with the driving force, this yields once again a diffusive-type dynamics, with  $D_2 \sim \eta_w / \rho$ . We recognize here the momentum diffusivity of water, a quantity independent of not only the oil viscosity, but even of the system size, as seen in Fig. 2(d). This is also visible in Fig. 3(b), where we plot  $D$  against drop volume  $\Omega$  for different viscosities of infusion. While large drops spread slightly quicker than smaller ones,  $D$  roughly tripling when the volume is multiplied by a factor of 40, the dynamics becomes independent of volume at large oil viscosity. The regime of high oil viscosity deserves a more complete study, where LISs infused with even more viscous oils could be considered to understand more quantitatively this apparent convergence of spreading dynamics.

For the converse case of small oil viscosity, the coefficient of diffusivity also reaches a plateau [Figs. 2(d) and 3(a)], which corresponds to the (water) inertial limit already known on solids [3–6]. However, the oil in the LIS gets also entrained during spreading, so that the oil inertia might also matter. After momentum has diffused across the oil film, the oil inertial force scales as  $\rho V^2 hr$  (where the oil density  $\rho$  is taken comparable to that of water), which yields a constant velocity of spreading  $(\gamma/\rho h)^{1/2}$  after its balance with the driving force  $\gamma r$ . Neither this behavior nor the one when considering the inertia of both water and oil (for which we expect a regime intermediate between  $t^{1/2}$  and  $t^1$ ) is observed in our experiments. In order to understand why, we can compare both inertial forces,  $\rho r^3 V^2/R$  and  $\rho r h V^2$ , respectively. We expect water inertia to dominate oil inertia when  $r$  is larger than a quantity of order  $(Rh)^{1/2}$ , suggesting that the regime dominated by oil inertia might be observed at small  $r$  (that is, short time). This regime is expected to be more apparent if the drop radius  $R$  is increased, and we show in the Supplemental Material [17] that the diffusive-like regime can indeed be preceded by a regime of constant velocity for larger drops, with a characteristic velocity of 1 m/s, the magnitude of the speed  $(\gamma/\rho h)^{1/2}$ .

LISs are often viewed as slippery surfaces, which they are from the adhesion point of view, but not necessarily from the friction point of view. It was found here that oil always lowers the speed of spreading, compared to what can be observed on a solid [Fig. 2(c)]. Different regimes of spreading were identified as a function of the viscosity of the infusion. However, they remarkably preserve diffusive-like dynamics, despite their different physics, which contrasts with other interfacial flows where inertial and viscous regimes generally exhibit different scalings in time [2,6]. At low oil viscosity,  $\eta_o < (\rho\gamma h^2/R)^{1/2}$ , the spreading behavior asymptotically approaches that on a bare solid; at intermediate viscosity,  $(\rho\gamma h^2/R)^{1/2} < \eta < \rho\gamma h/\eta_w$ , drops spread with significant effective slip on the infused surface; for high viscosities,  $\eta_o > \rho\gamma h/\eta_w$ , drops spread on the infused liquid with a vanishing slip velocity. We can deduce scaling laws for the spreading time as a function of oil viscosity. In the first case, the spreading time  $\tau$  scales as  $R^2/D_0 \sim (\rho R^3/\gamma)^{1/2}$ , the usual inertio-capillary time of a drop with size  $R$ . In the second interval,  $\tau$  scales as  $R^2/D_1 \sim \eta_o R^2/\gamma h$ . This time, now a function of  $\eta_o$ , is not the trivial viscous time  $\eta_o R/\gamma$  of relaxation of a drop driven by surface tension; rather, it includes the texture geometry, showing that the spreading of water on a viscous LIS results from an interplay between the drop relaxation and the film response. In the third limit,  $\tau$  scales as  $\rho R^2/\eta_w$ , where the LIS is so viscous that the drop does not “feel” it, which erases the signature of the oil viscosity in time; instead, we get the time for a viscous boundary layer to invade the drop. It would be interesting to complete this study by looking at the opposite limit of a viscous liquid (such as glycerol) spreading on a nonviscous LIS. Then the kinetics could benefit from the lubricating effect of the subjacent layer, and LISs could behave as slippery surfaces from both adhesional and frictional viewpoints.

#### ACKNOWLEDGMENTS

We are grateful to D. Beilharz for providing the pictures in Fig. 1(a), and we thank A. Keiser and P. Baumli for help in designing the samples. This project has received funding from the European Union’s Horizon 2020 research and innovation program under the Marie Skłodowska-Curie Grant No. 722497. We finally thank the reviewers for fruitful comments and remarks.

- 
- [1] P. G. De Gennes, Wetting: Statics and dynamics, *Rev. Mod. Phys.* **57**, 827 (1985).
  - [2] J. H. Snoeijer and B. Andreotti, Moving contact lines: Scales, regimes, and dynamical transitions, *Annu. Rev. Fluid Mech.* **45**, 269 (2013).
  - [3] A. L. Bianco, C. Clanet, and D. Quéré, First steps of the spreading of a liquid droplet, *Phys. Rev. E* **69**, 016301 (2004).
  - [4] J. C. Bird, S. Mandre, and H. A. Stone, Short-Time Dynamics of Partial Wetting, *Phys. Rev. Lett.* **100**, 234501 (2008).

- [5] K. G. Winkels, J. H. Weijts, A. Eddi, and J. H. Snoeijer, Initial spreading of low-viscosity drops on partially wetting surfaces, *Phys. Rev. E* **85**, 055301(R) (2012).
- [6] B. B. J. Stapelbroek, H. P. Jansen, E. S. Kooij, J. H. Snoeijer, and A. Eddi, Universal spreading of water drops on complex surfaces, *Soft Matter* **10**, 2641 (2014).
- [7] L. Tanner, The spreading of silicone oil drops on horizontal surface, *J. Phys. D* **12**, 1473 (1979).
- [8] T. S. Wong, S. H. Kang, S. K. Tang, E. J. Smythe, B. D. Hatton, A. Grinthal, and J. Aizenberg, Bioinspired self-repairing slippery surfaces with pressure-stable omniphobicity, *Nature (London)* **477**, 443 (2011).
- [9] A. Lafuma and D. Quéré, Slippery pre-suffused surfaces, *EPL (Eur. Phys. Lett.)* **96**, 56001 (2011).
- [10] J. D. Smith, R. Dhiman, S. Anand, E. Reza-Garduno, R. E. Cohen, G. H. McKinley, and K. K. Varanasi, Droplet mobility on lubricant-impregnated surfaces, *Soft Matter* **9**, 1772 (2013).
- [11] F. Schellenberger, J. Xie, N. Encinas, A. Hardy, M. Klapper, P. Papadopoulos, H. J. Butt, and D. Vollmer, Direct observation of drops on slippery lubricant-infused surfaces, *Soft Matter* **11**, 7617 (2015).
- [12] S. Hardt and G. McHale, Flow and drop transport along liquid-infused surfaces, *Annu. Rev. Fluid Mech.* **54**, 83 (2022).
- [13] M. Tenjimbayashi, R. Togasawa, K. Manabe, T. Matsubayashi, T. Moriya, M. Komine, and S. Shiratori, Liquid-infused smooth coating with transparency, super-durability, and extraordinary hydrophobicity, *Adv. Funct. Mater.* **26**, 6693 (2016).
- [14] X. Yao, Y. Hu, A. Grinthal, T. S. Wong, L. Mahadevan, and J. Aizenberg, Adaptive fluid-infused porous films with tunable transparency and wettability, *Nat. Mater.* **12**, 529 (2013).
- [15] A. Keiser, L. Keiser, C. Clanet, and D. Quéré, Drop friction on liquid-infused materials, *Soft Matter* **13**, 6981 (2017).
- [16] J. H. Guan, E. R. Gutierrez, B. Xu, D. Wood, G. McHale, R. A. L. Aguilar, and G. G. Wells, Drop transport and positioning on lubricant impregnated surfaces, *Soft Matter* **13**, 3404 (2017).
- [17] See Supplemental Material at <http://link.aps.org/supplemental/10.1103/PhysRevFluids.7.084003> for related content and supplemental movies.
- [18] L. Courbin, E. Denieul, E. Dressaire, M. Roper, A. Ajdari, and H. A. Stone, Imbibition by polygonal spreading on microdecorated surfaces, *Nat. Mater.* **6**, 661 (2007).
- [19] H. Hasimoto, On the periodic fundamental solutions of the Stokes equations and their application to viscous flow past a cubic array of spheres, *J. Fluid Mech.* **5**, 317 (1959).
- [20] A. S. Sangani and A. Acrivos, Slow flow past periodic arrays of cylinders with application to heat transfer, *Int. J. Multiphase Flow* **8**, 193 (1982).
- [21] D. Daniel, J. V. Timonen, R. Li, S. J. Velling, and J. Aizenberg, Oleoplaning droplets on lubricated surfaces, *Nat. Phys.* **13**, 1020 (2017).
- [22] A. Keiser, P. Baumli, D. Vollmer, and D. Quéré, Universality of friction laws on liquid-infused materials, *Phys. Rev. Fluids* **5**, 014005 (2020).
- [23] J. D. Paulsen, J. C. Burton, and S. R. Nagel, Viscous to Inertial Crossover in Liquid Drop Coalescence, *Phys. Rev. Lett.* **106**, 114501 (2011).
- [24] A. Eddi, K. G. Winkels, and J. H. Snoeijer, Short time dynamics of viscous drop spreading, *Phys. Fluids* **25**, 013102 (2013).

*Correction:* Conversion errors in production resulted in some occurrences of the letters  $D$ ,  $R$ ,  $\gamma$ , and  $\eta$  to appear incorrectly. They have now been fixed. Minor errors in inline equations in the second sentence below Eq. (2) and in the fifth sentence of the fourth paragraph of Sec. V have been fixed.